

MAGNETIC PROPERTIES OF $TbCl_3$ DETERMINED BY NEUTRON SCATTERING*

A. MURASIK[†], P. FISCHER and A. FURRER

Laboratorium für Neutronenstreuung, CH-5303 Würenlingen (Switzerland)

W. SZCZEPANIAK

Institute of Inorganic Chemistry and Metallurgy of Rare Earths, Wrocław Technical University, 05-370 Wrocław (Poland)

(Received January 15, 1985)

Summary

Neutron diffraction measurements performed on polycrystalline $TbCl_3$ yield ferromagnetic long-range order below $T_C = (3.70 \pm 0.05)$ K and ordered magnetic moments with a magnitude of $(8.4 \pm 0.1) \mu_B$ per Tb^{3+} ion at saturation, aligned perpendicular to the c axis. Structural parameters were refined at 1.3, 4.2, and 293 K. By means of inelastic neutron scattering we have determined the crystal-field level scheme which is able to predict correctly both the observed anisotropy and zero-field magnetization of $TbCl_3$.

1. Introduction

The magnetic properties of rare-earth trihalides are of particular interest due to their low ordering temperatures and corresponding weak exchange interactions, which are comparable in magnitude to dipolar interactions [1 - 3]. While the hexagonal rare-earth trichlorides were a subject of extensive studies, there is a paucity of experimental data on the orthorhombic phases. In this series $TbCl_3$ appears to be the most attractive compound for studying the combined effects of dipolar and exchange coupling because of the large magnetic moment of the Tb^{3+} ions. This has been demonstrated for ferromagnetic $Tb(OH)_3$ (hexagonal $LaCl_3$ -type structure, $T_C = 3.72$ K) for which unusual cancellation effects between magnetic dipole and exchange interactions were found [4].

Terbium trichloride has the orthorhombic $PuBr_3$ -type structure with space group $Cmcm$, which is typical for tribromides and triiodides of rare

*Paper presented at the International Rare Earth Conference, ETH Zurich, Switzerland, March 4 - 8, 1985.

[†]Permanent address: Institute of Atomic Energy, 05-400 Otwock/Swierk, Poland.

earths and many actinides [5 - 7]. To our knowledge neither bulk magnetic measurements nor neutron scattering results have been published until now on this compound. By means of neutron scattering experiments performed on polycrystalline TbCl_3 in the temperature range 1.3 - 293 K, we determined the long-range magnetic order, the zero-field magnetization, and the crystal-field splitting of the ${}^7\text{F}_6$ ground state of the Tb^{3+} ion. The latter results provide a satisfactory interpretation of the magnetic properties of TbCl_3 .

2. Experimental details

2.1. Sample preparation

Anhydrous TbCl_3 was prepared according to standard methods [8, 9], which are based on the chlorination action of NH_4Cl during dehydration of the $\text{TbCl}_3 \cdot \text{H}_2\text{O}$ and NH_4Cl mixture. Tb_4O_7 (Johnson Matthey Chemicals Ltd., spec. pure) was dissolved in concentrated hydrochloric acid. Five-fold molar excess of NH_4Cl was then added and the solution was evaporated. The mixture of chlorides was placed in a quartz ampoule connected to the vacuum line and slowly heated under vacuum to 400 °C in order to remove the water and NH_4Cl . The temperature was then raised to 600 - 650 °C and anhydrous TbCl_3 was melted. Finally, the ampoule was sealed off under vacuum. All handling operations were made in a dry-box filled with Ar or He.

2.2. Neutron diffraction investigations

Approximately 15 g of TbCl_3 powder was sealed in a vanadium container of 15 mm diameter. Neutron diffraction patterns were measured on the powder diffractometer at the Saphir reactor, Würenlingen, in the temperature range 1.3 - 293 K using neutrons of wavelength 2.324 Å and a bath-type cryostat. During pumping the helium-bath temperature was maintained constant to within 5 mK by means of a vapor-pressure regulator. The temperature was measured by means of a calibrated germanium resistor. The Rietveld profile method [10] was used to analyse the neutron diagrams, based on the scattering lengths $b_{\text{Tb}} = 7.38$ fm and $b_{\text{Cl}} = 9.58$ fm [13]. The magnetic form factor of Tb^{3+} ($4f^6$) was taken in the dipole approximation [11].

Figure 1 shows characteristic neutron diffraction patterns at 4.2 K in the paramagnetic state and at 1.3 K for ferromagnetic TbCl_3 . Seventy-three inequivalent reflections (hkl) contribute to the profile intensities. The calculations were based on space group $Cmcm$ [5] with the following atomic positions: Tb and Cl(1) in 4(c): $\pm(0, y, \frac{1}{4})$ and Cl(2) in 8(f): $\pm(0, y', z'; 0, y', \frac{1}{2} - z') + \{0, 0, 0; \frac{1}{2}, \frac{1}{2}, 0\}$. Refined values of the structure parameters are summarized in Tables 1 and 2 and compared with previous X-ray results and isostructural UI_3 [12]. The observed and calculated diagrams are in fair agreement. Table 3 shows selected interatomic distances relevant to crystal-

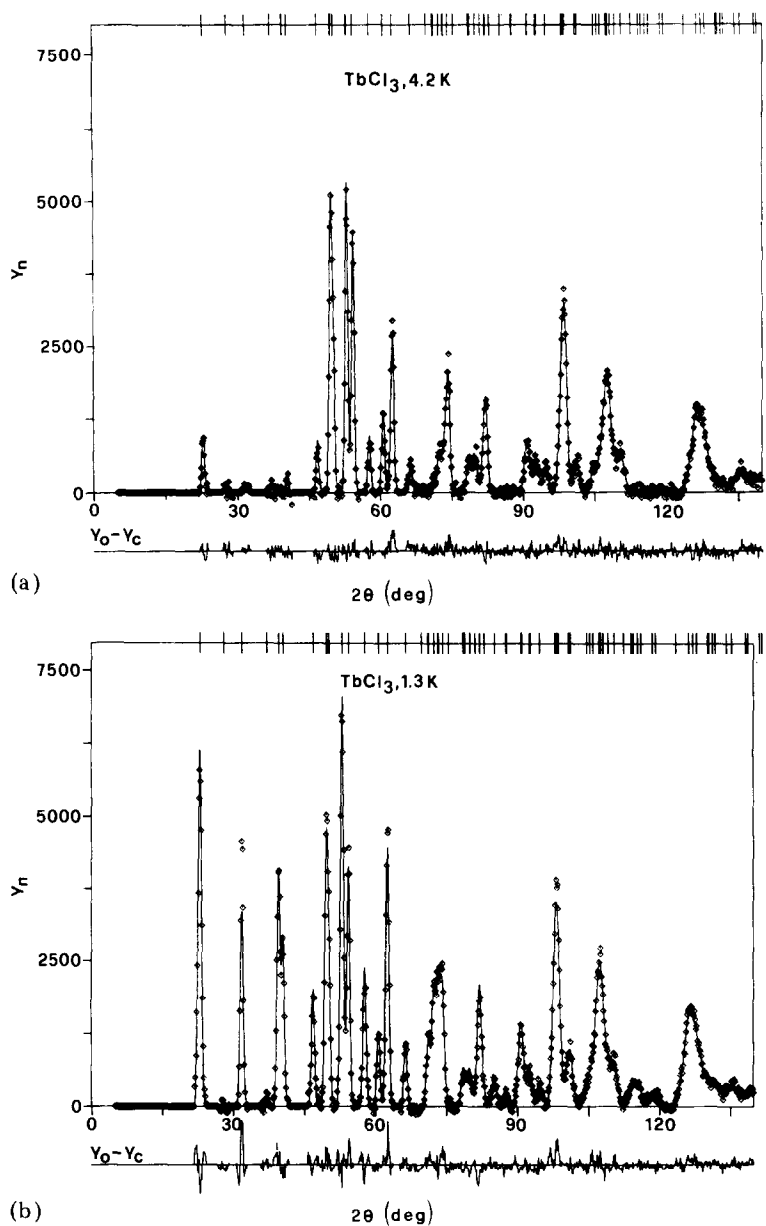


Fig. 1. (a) Observed (points, corrected for absorption and background) and calculated (line) neutron-diffraction patterns of paramagnetic TbCl_3 at 4.2 K. (b) Observed (points) and calculated (line) neutron-diffraction intensities of ferromagnetic TbCl_3 at 1.3 K.

field calculations. The coordination polyhedron in TbCl_3 is a bicapped trigonal prism in which the terbium ion is surrounded by eight chlorine ions.

Compared with the 4.2 K diagram, the neutron diffraction pattern measured at 1.3 K (see Fig. 1) clearly indicates large magnetic contributions

TABLE 1

Lattice constants of TbCl_3 , compared with UI_3 [12]

Compound	T (K)	a (Å)	b (Å)	c (Å)
TbCl_3^a	293	3.86(2)	11.71(3)	8.48(3)
TbCl_3	293	3.847(2)	11.771(5)	8.516(4)
TbCl_3	4.2	3.849(2)	11.680(5)	8.482(4)
TbCl_3	1.3	3.848(2)	11.679(5)	8.481(4)
UI_3	4.2 [13]	4.324(6)	13.93(2)	9.94(1)

Estimated standard deviations correspond to the last digit.

^aX-ray results obtained by Forrester *et al.* [5]

except for the $h00$ reflections. No superstructure peaks were detected. Hence, the magnetic and nuclear unit cells coincide. These observations may be explained on the basis of long-range ferromagnetic ordering with magnetic moments approximately aligned along the a axis. Direction (100) is parallel to the orientations of magnetic moments of uranium ions in isostructural, antiferromagnetic UI_3 [12]. However, the best agreement of observed and calculated intensities of TbCl_3 at 1.3 K ($R_{\text{Im}} = 5.5\%$, see Table 2) is obtained for magnetic moment components $\mu_x = 7.9(1) \mu_B$, $\mu_y = 3.1(2) \mu_B$, $\mu_z = 0$, *i.e.*, $\mu_{\text{Tb}} = 8.4(1) \mu_B$. On the other hand, the assumption $\mu = \mu_x$ yields $\mu_{\text{Tb}} = 8.2(1) \mu_B$ and $R_{\text{Im}} = 7.5\%$ ($R_{\text{In}} = 6.1\%$, $R_{\text{wp}} = 13.9\%$). Figure 2 shows the temperature dependence of the zero-field magnetization which yields the ordering temperature $T_C = (3.70 \pm 0.05)$ K. At 1.3 K the ordered magnetic moment reaches saturation.

2.3. Inelastic neutron scattering measurements

Inelastic neutron scattering experiments were carried out for a polycrystalline sample of TbCl_3 sealed in a cylindrical Al container of 15 mm diameter in order to obtain information on the crystal-field level scheme of the $^7\text{F}_6$ ground state of the Tb^{3+} ions. The measurements were performed on a triple-axis spectrometer at the Saphir reactor at Würenlingen in the neutron energy-loss configuration. The scattered-neutron energy was fixed at 13.7 meV, and a graphite filter was used to remove higher-order contamination. Energy spectra were taken at various temperatures and moduli of the scattering vector Q for energy transfer up to 65 meV.

Typical energy spectra are shown in Fig. 3. There is not much structure in the observed spectra except for the strong inelastic line at around 16 meV which is undoubtedly of magnetic origin. In addition there is a broad maximum centered at around 25 meV which can be identified as phonon scattering; for $\hbar\omega > 30$ meV no further peaks have been observed.

The present data do not allow a detailed analysis of the observed energy spectra in terms of the crystal-field Hamiltonian:

TABLE 2
 Temperature dependence of structure parameters ($\times 10^4$) of TbCl_3 in comparison to UCl_3 [12]

Compound	T (K)	$y_{\text{Tb}}(\text{U})$	$y_{\text{Cl}}(\text{I})$	$y'_{\text{Cl}}(\text{I})$	$z'_{\text{Cl}}(\text{I})$	B (\AA^2)	R_{wp}	R_{In}	R_{Im}	R_e
TbCl_3^{a}	293	2440(10)	5830(30)	1450(20)	5690(20)					
TbCl_3	293	2433(5)	5851(3)	1474(3)	5670(4)	1.36(5)	0.103	0.047	—	0.041
TbCl_3	4.2	2458(6)	5857(4)	1466(3)	5664(5)	0.32(7)	0.132	0.055	—	0.062
TbCl_3	1.3	2436(7)	5858(6)	1473(5)	5663(7)	0.32	0.128	0.054	0.055	0.045
UCl_3	4.2 (12)	2426(7)	5744(7)	1437(6)	5645(6)					

B , Debye-Waller parameter.

R_{wp} , R_{In} , R_{Im} : reliability factors for weighted profile, integrated nuclear and magnetic intensities, respectively.

R_e , statistically expected value.

^aX-ray results obtained by Forrester *et al.* [5].

TABLE 3

Shortest interatomic distances for TbCl_3 calculated from the parameters summarized in Tables 1 and 2, compared with UI_3 [12]

Bond	Distances (\AA) in TbCl_3 at temperature (K)				Distances (\AA) in UI_3 at 4.2 K
	1.3	4.2	293	293 ^a	
Tb-Tb (2 \times) (U-U)	3.848(2)	3.849(2)	3.847(2)	3.86(2)	4.324(6)
Tb-Cl1 (2 \times) (U-II)	2.664(7)	2.684(6)	2.677(5)	2.70(2)	3.19(1)
Tb-Cl2 (4 \times) (U-I2)	2.784(5)	2.776(4)	2.790(4)	2.79(2)	3.254(7)
Tb-Cl2 (2 \times) (U-I2)	2.908(6)	2.923(5)	2.926(4)	2.95(2)	3.417(8)
Tb-Cl1 (1 \times) (U-II)	4.00(1)	3.970(9)	4.023(7)	3.97(3)	4.62(1)
Cl-Cl (I-I)	3.378(5)	3.378(4)	3.395(3)	3.07(4)	3.69(1)

^aX-ray results obtained by Forrester *et al.* [5].

$$\hat{\mathcal{H}} = \sum_{n=1}^3 \sum_{m=0}^n B_{2n}^{2m} \hat{O}_{2n}^{2m} \quad (1)$$

which contains nine independent crystal-field parameters, B_{2n}^{2m} . However, from general experience with crystal-field problems the ratios of the crystal-field parameters for a particular degree n may reasonably be determined by taking account of the geometry of the coordination polyhedron formed by the eight nearest chlorine neighbours, as listed in Table 3. We find:

$$\begin{aligned} B_2^2 &= -1.271B_2^0; \\ B_4^2 &= -3.752B_4^0, B_4^4 = 1.162B_4^0; \\ B_6^2 &= 0.858B_6^0, B_6^4 = 3.939B_6^0, B_6^6 = -9.531B_6^0 \end{aligned} \quad (2)$$

Using these constraints we are left with three independent crystal-field parameters B_2^0 , B_4^0 , B_6^0 . In order to cover all possible values of the ratios B_4^0/B_2^0 and B_6^0/B_4^0 we used the following parametrization scheme:

$$\frac{B_4^0}{B_2^0} = \frac{30xy}{1-|y|}, \quad \frac{B_6^0}{B_4^0} = \frac{x}{126(1-|x|)}, \quad (3)$$

with $-1 \leq x \leq 1$ and $-1 \leq y \leq 1$. Since reliable information on the crystal-field parameters of TbCl_3 is lacking, we diagonalized the Hamiltonian (1) for all possible combinations of the parameters x and y . In the analysis of the resulting level schemes only parameter sets giving a predominantly $|J_z\rangle = |\pm 6\rangle$ ground state have been retained, because the observed zero-field magnetization is close to its maximum value of $9 \mu_B$ at low temperatures. This

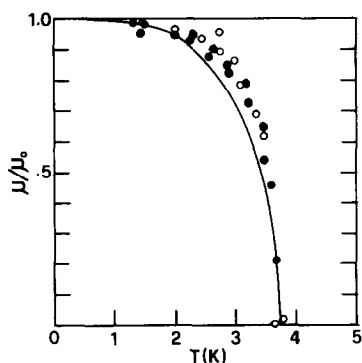


Fig. 2. Zero-field magnetization of ferromagnetic TbCl_3 . Open and closed circles correspond to reflections 020 and 002, respectively. The solid line represents the calculated zero-field magnetization as described in the text.

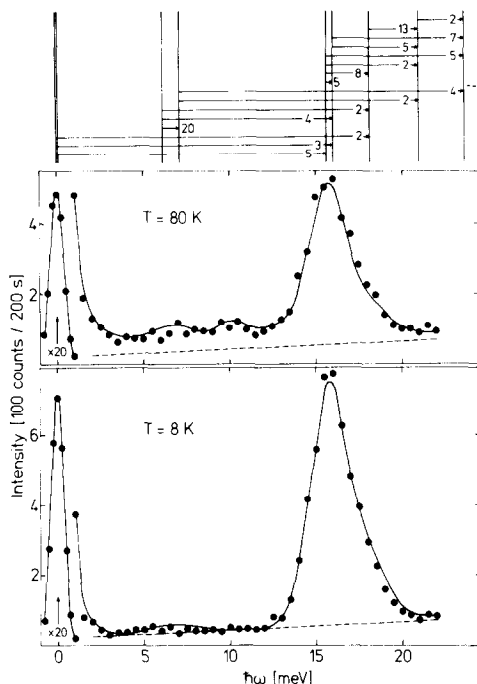


Fig. 3. Energy spectra of neutrons scattered from polycrystalline TbCl_3 for $Q = 1.95 \text{ \AA}^{-1}$. The solid lines correspond to the calculated energy spectra as described in the text. The background level is indicated by the dashed line. The top of the Figure shows the resulting crystal-field level scheme. The arrows denote the allowed crystal-field transitions with matrix elements $\langle n | \hat{J}_\perp | m \rangle^2 \geq 1$, which are indicated for each transition.

procedure considerably limited the possible level schemes, which were then compared in detail with the observed energy spectra. Finally, we arrived at a unique parameter set which correctly reproduced both the asymmetric shape of the line at 16 meV, and the intensity increase in the low-energy region upon raising the temperature from 8 K to 80 K. The resulting parameters are:

$$B_2^0 = (-7.6 \pm 0.8) \times 10^{-2} \text{ meV}$$

$$B_4^0 = (-2.3 \pm 0.3) \times 10^{-3} \text{ meV}$$

$$B_6^0 = (1.2 \pm 0.4) \times 10^{-5} \text{ meV}$$

giving rise to $\chi^2 = 5$ (where χ^2 is the mean deviation of the calculated energy spectra from those observed). No other parameter set was able to reproduce the experimental data equally well; in fact, the second-best fit yielded $\chi^2 = 20$. The resulting crystal-field level scheme is indicated above Fig. 3 (except for the four highest-excited crystal-field levels between 35 meV and 42 meV, which do not contribute to the scattering below $T = 100 \text{ K}$).

3. Conclusion

Our analysis of the observed energy spectra shows that the crystal-field ground state corresponds to an "accidental" doublet composed mainly of a nearly pure symmetric and antisymmetric combination of $|J_z\rangle = |\pm 6\rangle$. The next excited levels are far above the ground state; thus the magnetic properties of TbCl_3 at low temperatures are essentially determined by the two ground-state singlets separated by less than 0.1 meV. Calculations of the zero-field magnetization, in which the molecular-field parameter was chosen to predict correctly the observed ordering temperature, $T_C = 3.7$ K, proved that the crystal-field anisotropy constrains the magnetic moments to lie perpendicular to the c -axis with a value of $8.6 \mu_B$ at 1.3 K, which is very close to the observed zero-field magnetization.

TbCl_3 exhibits, in many aspects, the magnetic properties found in $\text{Tb}(\text{OH})_3$ [4] for which estimates of the interactions between first-, second- and third-nearest neighbours reveal unusual cancellations between the magnetic dipole and exchange interactions. In consequence, the net interaction becomes comparable with the long-range dipole interactions. For a more detailed analysis of the magnetic properties of TbCl_3 , however, single-crystal studies are required.

Acknowledgments

We are indebted to H. Heer for making available the RESTA program. One of us (A.M.) gratefully acknowledges the financial support provided by the ETH, Zurich.

References

- 1 J. C. Eisenstein, R. P. Hudson and B. W. Magnum, *Phys. Rev. A*, **137** (1965) 1886.
- 2 J. H. Colwell, B. W. Magnum and D. B. Utton, *Phys. Rev.*, **181** (1962) 842.
- 3 J. Felsteiner and S. K. Misra, *Phys. Rev. B*, **8** (1973) 253.
- 4 C. A. Catanese, A. T. Skjeltop, H. E. Meissner and W. P. Wolf, *Phys. Rev. B*, **8** (1973) 4223.
- 5 J. D. Forrester, A. Zalkin, D. H. Templeton and J. C. Wallmann, *J. Chem. Phys.*, **3** (1964) 185.
- 6 J. C. Taylor, *Coord. Chem. Rev.*, **20** (1976) 197.
- 7 J. M. Haschke, in K. A. Gschneidner, Jr. and L. Eyring (eds.), *Handbook on the Physics and Chemistry of Rare Earths*, Vol. 4, North-Holland, Amsterdam, 1979, p. 89.
- 8 M. D. Taylor and C. P. Carter, *J. Inorg. Nucl. Chem.*, **24** (1962) 387.
- 9 M. D. Taylor, *Rev. Chem.*, **62** (1962) 503.
- 10 H. M. Rietveld, *J. Appl. Crystallogr.*, **2** (1969) 65.
- 11 A. J. Freeman, J. P. Desclaux, G. H. Lander and J. Faber, Jr., *Phys. Rev. B*, **13** (1976) 1168.
- 12 A. Murasik, P. Fischer and W. Szczepaniak, *J. Phys. C*, **14** (1981) 1847.